Plasmonic Harvesting of Light Energy for Suzuki Coupling Reactions

Feng Wang,[†,‡] Chuanhao Li,[§,‖] Huanjun Chen,[‡] Ruibin Jiang,[‡] Ling-Dong Sun,*[†] Quan Li,[‡] Jianfang Wang,*[‡] Jimmy C. Yu,[§] and Chun-Hua Yan*[†]

[†]State Key Lab of Rare Earth Materials Chemistry and Applications, Peking University, Beijing 100871, China

[‡]Department of Physics, The Chinese University of Hong Kong, Shatin, Hong Kong SAR, China

[§]Department of Chemistry, The Chinese University of Hong Kong, Shatin, Hong Kong SAR, China

[‖]School of Chemistry and Chemical Engineering, Anhui University, Hefei 230039, Anhui, China

Ⓢ *Supporting Information*

ABSTRACT: The efficient use of solar energy has received wide interest due to increasing energy and environmental concerns. A potential means in chemistry is sunlight-driven catalytic reactions. We report here on the direct harvesting of visible-to-near-infrared light for chemical reactions by use of plasmonic Au–Pd nanostructures. The intimate integration of plasmonic Au nanorods with catalytic Pd nanoparticles through seeded growth enabled efficient light harvesting for catalytic reactions on the nanostructures. Upon plasmon excitation, catalytic reactions were induced and accelerated through both plasmonic photocatalysis and photothermal conversion. Under the illumination of an 809 nm laser at 1.68 W, the yield of the Suzuki coupling

reaction was ∼2 times that obtained when the reaction was thermally heated to the same temperature. Moreover, the yield was also ∼2 times that obtained from Au–TiO$_x$–Pd nanostructures under the same laser illumination, where a 25-nm-thick TiO$_x$ shell was introduced to prevent the photocatalysis process. This is a more direct comparison between the effect of joint plasmonic photocatalysis and photothermal conversion with that of sole photothermal conversion. The contribution of plasmonic photocatalysis became larger when the laser illumination was at the plasmon resonance wavelength. It increased when the power of the incident laser at the plasmon resonance was raised. Differently sized Au–Pd nanostructures were further designed and mixed together to make the mixture light-responsive over the visible to near-infrared region. In the presence of the mixture, the reactions were completed within 2 h under sunlight, while almost no reactions occurred in the dark.
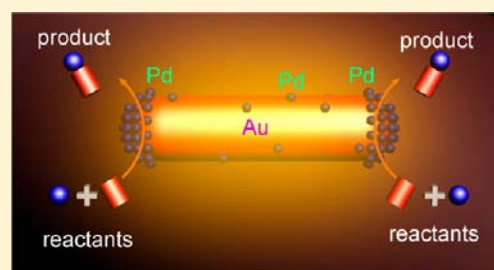
1. INTRODUCTION

Solar energy is of great potential as a clean, abundant, and economical energy source. Efficient harvesting of solar energy is promising and has been a worldwide high priority target.[1] Up to date, there have been three primary solar energy technologies: solar heating, solar photovoltaics, and solar thermal electricity.[2,3] They are mainly used for solar-to-electricity conversion and solar water heating. Besides these technologies, the exploration of new solar energy harvesting means is also important and will have long-term impacts. The use of sunlight to drive chemical reactions[4,5] is one of these new approaches. It can be potentially applied to various industrial chemical processes. Solar-driven chemical reactions can be realized through photocatalysis, such as photocatalytic water splitting,[6,7] where semiconductors are typically utilized and photogenerated electrons/holes reduce/oxidize water to produce H$_2$/O$_2$, or by recently reported plasmon-assisted chemical reactions.[8]

Localized plasmon resonances refer to the collective electron oscillations in noble metal nanocrystals caused by interaction with light. Excited plasmon resonances can greatly enhance the electric field near the nanocrystal surface. Plasmon-enhanced electric fields play an essential role in surface-enhanced spectroscopies.[9] The excited oscillations of electrons are relaxed

rapidly, on the order of femtoseconds, through electron–electron scattering, resulting in a Fermi–Dirac redistribution of energetic electrons at a higher temperature.[10] The presence of energetic or hot electrons upon plasmon excitation has recently been corroborated by the detection of a photocurrent through a plasmonic metal–semiconductor Schottky junction.[11] The photocurrent has been ascribed to the injection of the hot electrons over the Schottky barrier. Hot electrons generated by plasmon excitation cool down through electron–phonon interactions at a time scale of 1–100 ps,[10] causing a rise in the lattice temperature of the metal nanocrystal. This thermal energy is thereafter dissipated to the surrounding medium, leading to plasmonic photothermal conversion.

Several different mechanisms have been discovered in plasmon-enhanced chemical reactions. Plasmon-enhanced electric fields can focus light in the region close to semiconductor nanostructures, increase their light absorption, and thus improve their photocatalytic activities.[12−16] Plasmon excitation can also cause electrons from plasmonic nanocrystals to be injected into the conduction band of semiconductors, thus leading to electron–hole separation. The plasmonic

nanocrystal then serves as an anode to conduct oxidizing reactions while the semiconductor functions as a cathode to induce reducing reactions.[17−21] The plasmon excitation-induced electron injection from plasmonic nanocrystals to semiconductors can be considered as a plasmonic sensitization process.

Both plasmonic enhancement of light absorption and plasmonic sensitization have mostly replied on traditional semiconductors, where plasmonic nanocrystals function as either light antennas or sensitizers. On the other hand, direct interactions between plasmonic nanocrystals and reactive molecules have also been realized,[8] which can be regarded as plasmonic photocatalysis. A possible interaction manner is the direct injection of the excited hot electrons from plasmonic nanocrystals into the antibonding orbitals of adsorbed molecules.[22−24] The occupation of the antibonding orbitals will weaken the related bonds and lead to desired reactions. Plasmonic photocatalysis has been demonstrated in the use of Au nanocrystals to drive the oxidation of formaldehyde and methanol[22] and the reduction of nitroaromatic compounds[23] at moderate temperatures. Moreover, plasmonic photothermal conversion has also been employed to enhance chemical reactions[25,26] because reaction rates are dependent exponentially on temperature. Plasmonic photothermal conversion has been widely studied and employed in various optical and biotechnological applications.[27−33] For chemical reactions, the photothermal heating of Au and Ag nanocrystals has been utilized to increase the reaction rate between hexacyanoferrate-(III) and thiosulfate in solutions[25] and the steam reforming reaction rate between ethanol and water on microfluidic chips.[26] In addition, the plasmonic photocatalysis and photothermal heating of Au and Ag nanocrystals have also been found to take effect jointly in the acceleration of CO oxidation[34] and ethylene epoxidation.[24]

The results from the studies mentioned above demonstrate clearly the possibility of using plasmonic metal nanocrystals as energy converters and catalysts to drive chemical reactions at moderate temperatures. However, the practical uses of plasmons to enhance chemical reactions require thorough investigations and understanding of the involved physical and chemical factors. On the one hand, the determination and quantification of the relative contributions of plasmonic photocatalysis and photothermal heating have remained elusive. On the other hand, in comparison to the traditional metal catalysts widely used in the chemical industry, such as palladium and platinum,[35−37] the catalytic properties of popular plasmonic Au and Ag nanocrystals have been less developed. Therefore, single-component plasmonic Au and Ag nanocrystals can only drive a limited range of chemical reactions. In addition, the ultimate goal of plasmon-enhanced reactions is to directly harvest solar energy for reactions, which has yet to be demonstrated.

In order to simultaneously achieve efficient light utilization and high catalytic activities, an intimate integration of strongly light-absorbing plasmonic and highly catalytically active components is strongly desirable. Such integration can also allow the light energy harvested by the plasmonic component to be directly utilized by the catalytic component. In this work, we designed Au−Pd nanostructures for the realization of the desired integration. Each nanostructure is composed of a Au nanorod decorated with multiple Pd nanoparticles. Au nanorods possess large extinction cross sections and have synthetically tunable longitudinal plasmon wavelengths cover-

ing the entire solar spectrum.[38−40] They can therefore function as the light-harvesting component. Pd nanoparticles are excellent catalysts for a variety of chemical reactions.[35,37] The Pd nanoparticles in our study are tightly attached to individual Au nanorods through heteroepitaxial growth.[41,42] Therefore, the chemical potentials of the electrons in the Pd nanoparticles and the Au nanorod are in equilibrium.[43] The plasmon resonance in the entire nanostructure also involves the electrons in the Pd nanoparticles. Illumination at an appropriate wavelength excites the plasmon resonance of the nanostructure. The plasmon excitation enables and accelerates the Pd-catalyzed Suzuki coupling reaction through plasmonic photo-catalysis and photothermal heating. A similar structure with a 25-nm-thick TiO_x shell to separate the Au core and Pd nanoparticles was also prepared. The TiO_x shell prevents the electronic interaction between the Au core and Pd nano-particles, and therefore prohibits the plasmonic photocatalysis process. The comparison between the catalytic performances of the Au−Pd nanostructures and the Au−TiO_x−Pd ones under light illumination confirms the contribution of plasmonic photocatalysis in the plasmon-enhanced Suzuki coupling reactions. An 809 nm laser was first used to verify the working principle, find out the reaction conditions, and ascertain the contributions of plasmonic photocatalysis and photothermal heating to the reaction yield. On the basis of the obtained findings, a mixture of Au−Pd nanostructures with different plasmon wavelengths was further contrived to demonstrate direct harvesting of sunlight for chemical reactions by matching the light-responsive spectrum of the mixture with the solar spectrum.

In comparison to previous experiments, our approach is superior in four aspects for plasmon-enhanced chemical reactions: (1) Synthetically tunable absorption wavelengths of plasmonic components allow for easy and efficient harvesting of light energy; (2) Intimate integration of plasmonic nanocrystals and catalytic nanoparticles offers the potential of studying a wide variety of industrially important reactions, raising the possibility of large-scale sunlight-driven chemical reactions in the chemical industry; (3) In comparison to semiconductor photocatalysis, the excited electrons in plasmonic metal nanostructures are confined in the surface region and thus need to travel only a very short distance to reaction sites; (4) Plasmonic photocatalysis is confirmed through the comparison between the catalytic activities of the Au−Pd nanostructures and the Au−TiO_x−Pd ones.

2. EXPERIMENTAL SECTION

2.1. Preparation of the Au−Pd Nanostructures. Five Au−Pd nanostructures were prepared. Four had Au nanorods, and one had Au nanospheres as cores. The five samples were named as large, medium, small, smallest, and spherical Au−Pd nanostructures, respectively. They were all prepared by a two-step seeded-growth method in aqueous solutions. The starting Au nanorod sample for the large nanostructures had a longitudinal plasmon wavelength of 760 nm. Its extinction value at 760 nm was 1.75 when measured with a 0.5 cm cuvette. They were grown in the first step following a reported procedure.[39] For the preparation of the large Au−Pd nanostructures in the second step, the as-grown Au nanorod solution (10 mL) was added into a growth solution composed of cetyltrimethylammonium chloride (CTAC, 30.3 mL, 0.025 M), H_2PdCl_4 (0.1 mL, 0.01 M), and ascorbic acid (0.05 mL, 0.1 M). The obtained solution was mixed by repeated gentle inversion for 10 s and then left undisturbed overnight at room temperature. The resultant Au−Pd nanostructure solution was
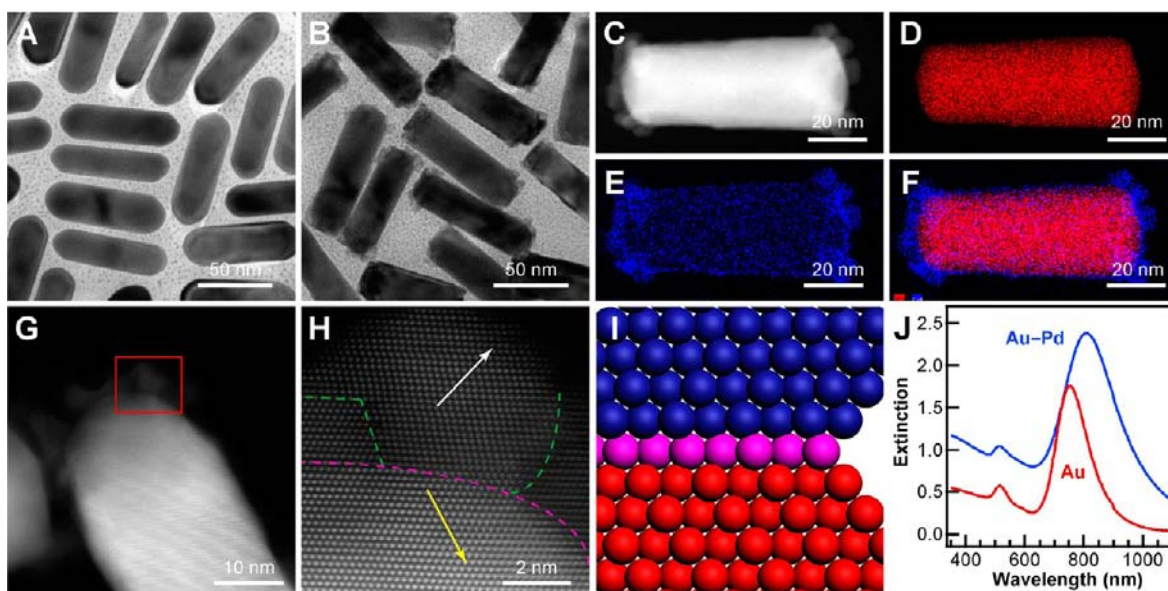
Figure 1. Large Au−Pd nanostructures. (A) TEM image of the original Au nanorods. (B) TEM image of the large nanostructures. (C) HAADF-STEM image of a single nanostructure. (D) Elemental map of gold on the nanostructure shown in C. (E) Corresponding elemental map of palladium. (F) Merged map. (G) HAADF-STEM image of another Au−Pd nanostructure. (H) Atomic-resolution HAADF-STEM image of the region indicated with a red rectangle in G. The pink dashed line indicates the edge of the Au nanorod. The green dashed line indicates the grain boundaries between Pd nanoparticles. The yellow and white arrows indicate the [110] direction of the face-centered-cubic Au and Pd lattices, respectively. (I) Schematic showing the (11−1) interface between the Au and Pd regions indicated with the arrows in (H). The red, blue, and pink spheres represent Au atoms, Pd atoms, and the atoms at the interface, respectively. (J) Extinction spectra. The extinction spectrum of the Au nanorods was obtained from the as-grown sample in a 0.5 cm cuvette, and that of the large Au−Pd nanostructures was recorded from the reaction solution in a 1 cm cuvette. The extinction value of the large nanostructure sample is 2.37 at 809 nm.

centrifuged at 6300 g for 10 min, and the precipitate was redispersed into water (2 mL) for catalytic reactions.

For the growth of the medium and small nanostructures, the same Au nanorod sample employed for the preparation of the large nanostructures were first subjected to oxidation[39] by adding HCl (0.2 mL, 1.0 M) in the as-grown nanorod solution (45 mL), followed by bubbling O_2 for 30 min. The solution was transferred into an isothermal oven at 65 °C. The oxidation process was monitored by measuring the extinction spectra from time to time. When the longitudinal plasmon wavelength reached 620 nm, the oxidation process was stopped by centrifugation. The precipitate was redispersed in water (45 mL). The same oxidation procedure was followed to make another Au nanorod sample with a longitudinal plasmon wavelength of 580 nm. The medium and small nanostructures were thereafter prepared using the oxidized Au nanorods (10 mL) as the seeds. The added H_2PdCl_4 (0.01 M) was changed to 0.05 mL. The Au−Pd nanostructure solutions were centrifuged and redispersed into water (1 mL) for catalytic reactions.

The growth procedure for the smallest nanostructures was the same as that for the large nanostructures, except that a Au nanorod sample with a smaller average diameter was used. The nanorod sample had a longitudinal plasmon wavelength of 760 nm. Its extinction value at 760 nm was 1.77 when measured in a 0.5 cm cuvette.

The growth procedure of the spherical nanostructures was the same as that for the small nanostructures, except that a Au nanosphere sample was used.[41] The Au nanosphere sample had a plasmon wavelength of 540 nm. Its extinction value at 540 nm was 0.38 when measured in a 0.5 nm cuvette.

2.2. Preparation of the Au−TiO$_x$−Pd Nanostructures. The Au−TiO$_x$ core−shell nanostructures were prepared following a reported method.[44] The same Au nanorod sample as in the preparation of the large Au−Pd nanostructures was employed. The as-grown Au nanorod solution (5 mL) was first added into a poly(sodium 4-styrenesulfonate) solution (PSS, MW 7 × 10^4 g·mol^{-1}, 5 mL, 2 g·L^{-1}, containing 6 mM NaCl), followed by stirring for 4 h. The solution was then centrifuged at 6300 g for 10 min. The

precipitate was redispersed into water (200 μL). To coat a TiO$_x$ shell, a TiCl$_3$ solution (200 μL, 17.1 wt %, containing 1.8 M HCl) was added into water (6 mL). The use of TiCl$_3$ is because it is much less reactive than TiCl$_4$, and its reactivity can be controlled by pH. NaHCO$_3$ solution (1.2 mL, 1.0 M) was then added dropwise into the above mixture, followed by the addition of the PSS-coated Au nanorod solution. After the mixture was stirred for 30 min, it was centrifuged at 6300 g for 10 min. The precipitate was thereafter added into a Pd seed solution (5 mL), which was prepared according to our reported procedure.[45] The resultant mixture was kept under ultrasonication for 1 h. The mixture was subsequently added into a growth solution made of CTAC (15 mL, 0.025 M), H_2PdCl_4 (0.1 mL, 0.01 M), and ascorbic acid (0.05 mL, 0.1 M). The obtained solution was mixed by repeated gentle inversion for 10 s and then left undisturbed overnight at room temperature. The resultant Au−TiO$_x$−Pd nanostructure solution was centrifuged at 6300 g for 10 min. The precipitate was redispersed into water (1 mL) for catalytic reactions.

For the growth of other Au−TiO$_x$−Pd nanostructures, the volumes of the Pd seed solution were changed to 2.5 and 1.25 mL, and the volumes of H_2PdCl_4 solution were changed to 0.05 and 0.025 mL, respectively.

2.3. Suzuki Coupling Reactions under Laser Illumination. A continuous semiconductor laser diode (JENOPTIK, JUM2500/50/20, VDM0003, maximum optical power: 3 W) at 809 nm was utilized for illumination. Both the large and the smallest Au−Pd nanostructures were utilized for the catalytic reactions under the laser illumination. Fourteen Suzuki coupling reactions with different reactants were carried out in a quartz cuvette with an optical path length of 1 cm. The reaction between bromobenzene and m-tolylboronic acid is used as an example. Bromobenzene (8.4 μL, 0.08 mmol) was added to H_2O (1.5 mL) in the presence of m-tolylboronic acid (10.9 mg, 0.08 mmol), NaOH (10 mg, 0.25 mmol), cetyltrimethylammonium bromide (CTAB) (36 mg), and the Au−Pd nanostructure (0.5 mL) or Au−TiO$_x$−Pd nanostructure samples (0.5 mL). CTAB helps in bringing bromobenzene into the aqueous reaction solution. The mixture solution was kept under the illumination of the 809 nm laser. The

diameter of the laser beam in the solution was ~0.33 cm. The reaction product was extracted with CH_2Cl_2 and immediately analyzed by gas chromatography−mass spectrometry (GC-MS). The GC-MS analysis was performed on an HP 6890 GC system equipped with an HP 5973 mass-selective detector and an HP-5 MS capillary column. To examine the contribution of the leached palladium to the reaction yield, the solution after 20 min of the reaction was centrifuged. The supernatant was divided into two aliquots. One aliquot was subjected to the GC-MS analysis, and the other aliquot was placed in a water bath and reacted for another 20 min.

2.4. Suzuki Coupling Reactions under Solar Radiation. Fourteen Suzuki coupling reactions with different reactants were carried out in a 4-mL glass vial. As an example, bromobenzene (8.4 μL, 0.08 mmol) was added to H_2O (1.5 mL) in the presence of m-tolylboronic acid (10.9 mg, 0.08 mmol), NaOH (10 mg, 0.25 mmol), CTAB (36 mg), and the mixture of medium, small, and spherical nanostructure samples (1 mL in total, 0.33 mL for each). The reactions were preformed on the roof of a building at Shatin, Hong Kong on sunny days from 2 to 4 p.m. in May 2011.

2.5. Characterization of the Nanostructures. The transmission electron microscopy (TEM) imaging and electron diffraction (ED) measurements were carried out on an FEI F20 microscope. The atomic-resolution Z-contrast imaging and high-angle annular dark-field scanning transmission electron microscopy (HAADF-STEM) characterizations were performed using a double-corrected Titan microscope operated at 300 kV. The high-resolution (HR) TEM images and energy-dispersive X-ray elemental maps were acquired on a probe Cs-corrected Titan microscope that was operated at 200 kV and equipped with an FEI super-X detector. The X-ray diffraction (XRD) patterns were acquired on a Rigaku Smartlab diffractometer with Cu Kα radiation. The extinction spectra were taken with quartz cuvettes on a Hitachi U-3501 UV/visible/NIR spectrophotometer. The setup for measuring the photothermal conversion was the same as described in our previous work.[46] Inductively coupled plasma optical emission spectroscopy (ICP-OES) characterizations were performed on a PerkinElmer Optima 4300DV system.

2.6. Density Functional Theory Calculations. The density functional theory (DFT) calculations were performed using the program package DMol3 in Materials Studio of Accelrys Inc. The exchange correlation energy was calculated within the generalized gradient approximation. The density functional semicore pseudopotential method was employed for Pd and Br atoms. The valence electron functions were expanded into a set of numerical atomic orbitals by a double numerical basis set with polarization functions. All computations were carried out with spin polarization. The Pd (111) surface was simulated with a three-layer slab model with nine Pd atoms per layer representing a (3×3) surface unit cell and with a 10 Å vacuum region. The reciprocal space of the (3×3) unit cell was sampled with a $(3 \times 3 \times 2)$ k-point grid generated automatically using the Monkhors-Pack method.[47] Full geometry optimization was performed for all relevant adsorbates, while the bottom layer Pd atoms were fixed at the bulk-truncated positions at the experimentally determined lattice constant of 3.891 Å. Transition state searches were performed with the complete linear synchronous transit/quadratic synchronous transit method.[48] The convergence criterion for the transition state searches was set to 0.01 hartree/Å for the root-mean-square of atomic forces.

3. RESULTS AND DISCUSSION

3.1. Au−Pd Nanostructures. The morphology and crystalline structure of the five nanostructure samples are elucidated with the large one as an example (Figure 1). The average diameter and length of the large nanostructures are 25 ± 2 and 82 ± 6 nm, respectively. The smooth, nearly hemispherical ends of the original Au nanorods (Figure 1A) become rough after the growth of Pd nanoparticles, while the surface at the side of the nanorods remains relatively smooth (Figure 1B). The morphological change suggests that Pd

nanoparticles are successfully grown on the surface of the nanorod. This observation is confirmed by HAADF-STEM imaging and elemental mapping (Figure 1C−F), from which the size of the Pd nanoparticles is estimated to be ~3−5 nm. In addition, a thin Pd wetting layer is also seen on the surface of each Au nanorod. The thickness of the wetting layer is estimated through high-resolution elemental mapping to be ~0.5 nm (Figure S1, Supporting Information). Such a thickness corresponds to 2−3 monolayers of Pd atoms.
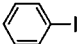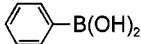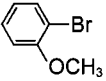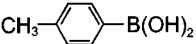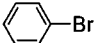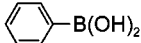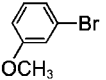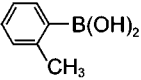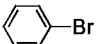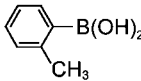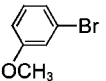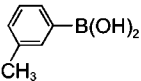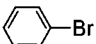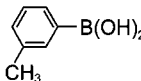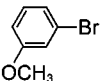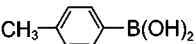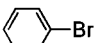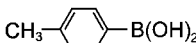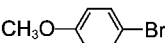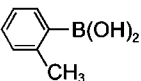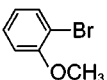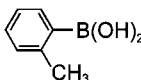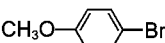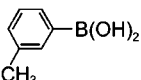
The atomic-resolution Z-contrast imaging of the large Au−Pd nanostructures indicates the lattice orientations of the Pd nanoparticles relative to that of the single-crystalline Au nanorod,[49] with an example shown in Figure 1G−I. The approximate edge of the nanorod is revealed by the HAADF-STEM image (Figure 1G). The left and right Pd nanoparticles (Figure 1H) assume the same lattice orientation as the Au nanorod, while the middle one exhibits a different lattice orientation. There exists an abrupt atomic interface between the middle Pd nanoparticle and the Au nanorod, with the atoms on the interfacial atomic layer shared by the Pd and Au lattices (Figure 1I). These observations indicate that the Pd nanoparticles are atomically bonded to the Au nanorod. The large Au−Pd nanostructures exhibit a strong longitudinal plasmon peak at 809 nm, while the longitudinal plasmon wavelength of the original Au nanorods is 760 nm (Figure 1J).

3.2. Suzuki Coupling Reactions under Laser Illumination. The Suzuki coupling reaction between bromobenzene and m-tolylboronic acid was used to examine the reaction conditions. The required reaction temperature with Pd-based catalysts is typically ~85 °C under isothermall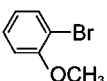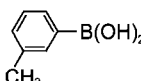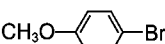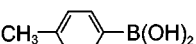y heating conditions.[50] The reaction was carried out in a 1 cm quartz cuvette using 0.5 mL of the large Au−Pd nanostructure sample (Figure S2, Supporting Information). ICP-OES measurements showed that the catalyst sample contained 81.5 μg of gold and 8.3 μg of palladium. The total amount of the metal was therefore 0.49 μmol. Under the illumination of an 809 nm laser at 1.68 W, the large Au−Pd nanostructures gave a yield of 99% in 1 h. The turnover frequency (TOF) was 0.045 s^{-1} if the total amount of the noble metal was considered and 0.28 s^{-1} if only the amount of palladium was considered. However, no product was generated without the laser illumination. We also added a mixture of the large Au nanorods and the separately prepared Pd nanocrystals (Figures S3 and S4, Supporting Information), with the Au and Pd molar compositions being equal to those of the large Au−Pd nanostructures in the reaction solution. The Pd nanocrystals are porous, and their catalytic activity for the Suzuki coupling reactions has been found to be size-independent.[45] Only a yield of 18% was obtained under the laser illumination at the same optical power. Furthermore, no product was obtained with either the porous Pd nanocrystals or the large Au nanorods under the laser illumination at the same power. These results indicate clearly that the Au−Pd nanostructures under the laser illumination enable the reaction. Moreover, the higher catalytic activity of the integrated Au−Pd nanostructures than that of the simple mixture verifies the importance of the intimate integration between plasmonic and catalytic components.

The above results demonstrate clearly that the Au−Pd nanostructures allow light energy to be efficiently utilized for chemical reactions. To examine its general applicability, we carried out the reactions with mono- and double-substituted aromatic halides and boronic acids using the same amount of the catalyst. Fourteen reactions were tested, with the yields

Table 1. Yields of the Suzuki Coupling Reactions in the Presence of the Large Au−Pd Nanostructures under the 809 nm Laser Illumination[a]

entry	halide	boronic acid	yield [%]	entry	halide	boronic acid	yield [%]
1	⬡–I	⬡–B(OH)₂	99	8	⬡–Br (OCH₃)	CH₃–⬡–B(OH)₂	94
2	⬡–Br	⬡–B(OH)₂	99	9	⬡–Br (OCH₃)	⬡–B(OH)₂ (CH₃)	43
3	⬡–Br	⬡–B(OH)₂ (CH₃)	99	10	⬡–Br (OCH₃)	⬡–B(OH)₂ (CH₃)	99
4	⬡–Br	⬡–B(OH)₂ (CH₃)	99	11	⬡–Br (OCH₃)	CH₃–⬡–B(OH)₂	99
5	⬡–Br	CH₃–⬡–B(OH)₂	94	12	CH₃O–⬡–Br	⬡–B(OH)₂ (CH₃)	59
6	⬡–Br (OCH₃)	⬡–B(OH)₂ (CH₃)	71	13	CH₃O–⬡–Br	⬡–B(OH)₂ (CH₃)	95
7	⬡–Br (OCH₃)	⬡–B(OH)₂ (CH₃)	80	14	CH₃O–⬡–Br	CH₃–⬡–B(OH)₂	99

[a]Large Au−Pd nanostructure solution, 0.5 mL; NaOH, 10 mg; CTAB, 36 mg; H₂O, 1.5 mL; reactant amounts of entries 1−5, 0.08 mmol halide and 0.08 mmol boronic acid; reactant amounts of entries 6−14, 0.04 mmol halide and 0.04 mmol boronic acid; laser power, 1.68 W; environment temperature, 25 °C; reaction time, 1 h.

Table 2. Yields of the Suzuki Coupling Reaction between Bromobenzene and *m*-Tolylboronic Acid in the Presence of the Large Au−Pd Nanostructures under the 809 nm Laser Illumination and Isothermal Heating

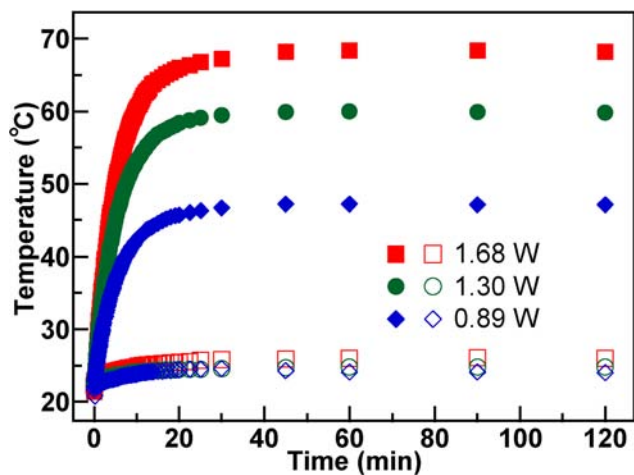| under the laser illumination[a]				under isothermal heating[b]		
laser power (W)	end temperature (°C)	photothermal conversion efficiency (%)	yield (%)	heating temperature (°C)	yield (%)	yield difference (%)
1.68	62	95.8	99	62	55	44
1.30	56	96.8	70	56	37	33
0.89	45	87.9	34	45	33	1

[a]Environmental temperature, 25 °C; reaction time, 20 min. [b]Reaction time, 20 min.

ranging from 43% to 99% (Table 1). The corresponding TOFs with respect to the total amount of the metal were also calculated (Table S1, Supporting Information). The yields of the Suzuki coupling reactions have been known to be dependent on the halide element, the positions and electron withdrawing/donating capabilities of the substitutional groups.[50] In our experiments, when active substrates, such as iodobenzene and bromobenzene, were used, yields of 99% were obtained (Table 1, entries 1−4). Moreover, yields of 71%, 43%, and 59% were obtained even when inactive substrates, such as *o*-tolylboronic acid, were supplied (Table 1, entries 6, 9, and 12). The rate-determining step of the reaction using bromobenzene or bromoanisole is the breaking of the C−Br bond.[51] In this step, electrons are transferred from Pd nanoparticles to the C and Br atoms to form C−Pd and Br−Pd bonds. We believe that the high yields that are obtained with inactive substrates arise from the plasmon-excitation-induced hot electrons on the metal catalyst. The hot electrons are higher in energy than the normal electrons and therefore are easier to inject into the adsorbed bromobenzene or bromoanisole molecules to break the C−Br bond.

3.3. Relative Contributions of Plasmonic Photocatalysis and Photothermal Heating. Plasmonic nanostructures can accelerate chemical reactions through both plasmonic photocatalysis and photothermal heating.[8,22−26,34] In order to ascertain whether the Suzuki coupling reactions were accelerated simply by the plasmonic heating of the reaction solutions or induced jointly by plasmon-excitation-derived hot electrons and photothermal heating, we performed control experiments for the coupling reaction between bromobenzene and *m*-tolylboronic acid under different circumstances. The control experiments were designed and divided into four categories: (1) photocatalysis (+) and photothermal heating (+), (2) photocatalysis (−) and photothermal heating (+), (3) photocatalysis (+) and photothermal heating (−), and (4) photocatalysis (−) and photothermal heating (−), where (+) and (−) mean that a mechanism is turned on and off respectively.

3.3.1. Photocatalysis (+) and Photothermal Heating (+). The reaction was illuminated by the 809 nm laser at different powers in an isothermal environment. The laser turned on both the photocatalysis mode and the photothermal heating mode. The yields were compared with those of the reaction heated to

the same temperatures in an isothermal water bath. The reaction yields were 99%, 70%, and 34% at the laser powers of 1.68, 1.30, and 0.89 W, respectively (Table 2). The reaction yield increases with the laser power. The temperatures of the reaction solution after the laser illumination for 20 min were also measured from the temperature rise traces[46] (Figure 2) to

be 62, 56, and 45 °C, respectively. From the temperature rise traces, the photothermal conversion efficiencies of the nanostructures (Table 2) can be determined, as described in detail in our previous work.[46] They are essentially the ratio of the absorbed light to the sum of the absorbed and scattered light. In addition, our previous study showed that the temperature in the reaction solution under our experimental conditions is spatially uniform under magnetic stirring.[46] The measured temperature rise traces and the obtained photothermal conversion efficiencies of the large Au−Pd nanostructures are similar to those of the pure Au nanorods of similar sizes.[46] The differences in the measured photothermal conversion efficiencies are ascribed to the time-dependent fluctuation in the temperature of the surrounding environment.

Figure 2. Temperature rise traces of the reaction solution at different powers of the 809 nm laser. The solid symbols are for the solution containing the large Au−Pd nanostructures, and the open symbols are for the solution without the metal nanostructures.

The temperatures of the isothermal water bath for directly heating the reaction solution were varied from 25 to 100 °C, with three of them being equal to the end temperatures reached under the laser illumination at the three different powers. The reaction yields in the water bath after 20 min were found to increase with temperature (Table S2, Supporting Information). No reaction occurred at 25 °C, suggesting that the Au−Pd nanostructures are catalytically inactive at room temperature. The reaction was complete within 20 min when the temperature reached 90 °C. The respective reaction yields were 55%, 37%, and 33% when the temperatures of the bath were equal to the end temperatures under the laser illumination (Table 2). The reaction yields in the bath are smaller than the corresponding ones under the laser illumination. The yield difference gets larger with increasing laser powers (Table 2). At 1.68 W, the yield difference reaches 44%. The results indicate
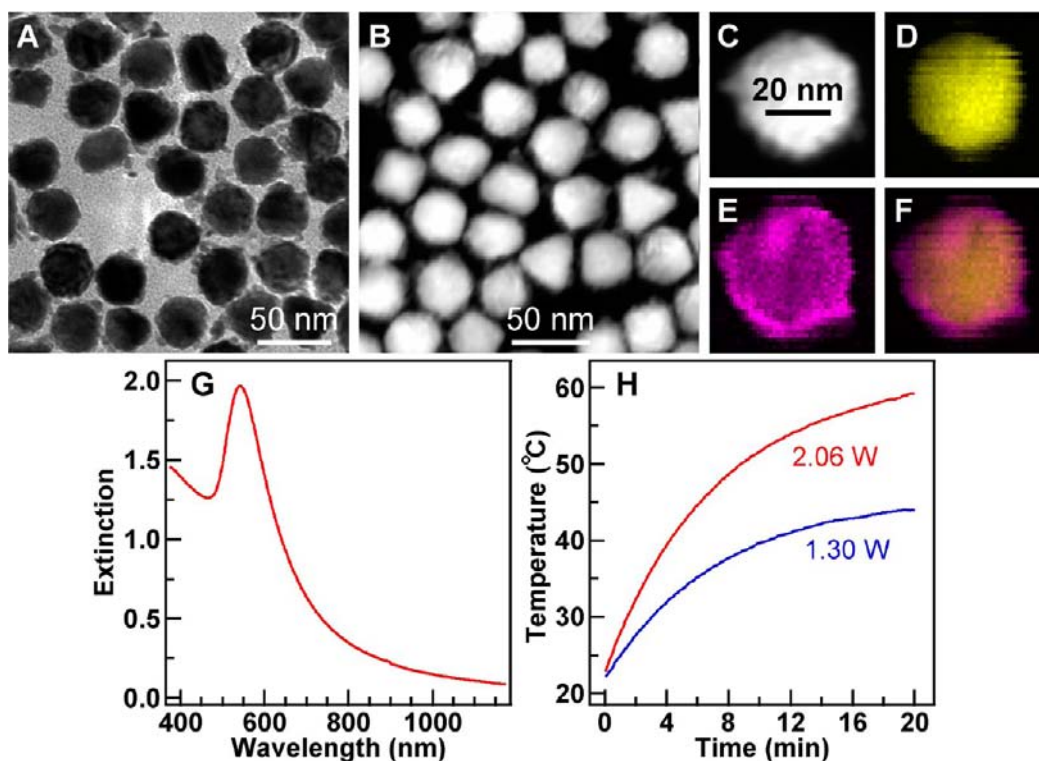
Figure 3. Spherical Au−Pd nanostructures. (A) TEM image. (B) HAADF-STEM image. (C) HAADF-STEM image of a single nanostructure. (D) Elemental map of gold of the nanostructure shown in C. (E) Corresponding elemental map of palladium. (F) Merged elemental map. (G) Extinction spectrum of the reaction solution containing the spherical nanostructures. The extinction value at 809 nm is 0.33 at a 1 cm path length. (H) Temperature rise traces of the reaction solution containing the spherical Au−Pd nanostructures at different laser powers. The temperatures were measured at a time interval of 5 s. Therefore the traces are shown as lines.

that the catalytic activity of the Au−Pd nanostructures under the laser illumination is contributed by both plasmonic heating process and plasmon-excitation-induced hot electrons. A rough estimation of the contribution of the hot electron effect, namely, plasmonic photocatalysis, can be made according to the reaction yields obtained under the isothermal heating relative to those under the laser illumination. The estimated percentages contributed by plasmonic photocatalysis are 44%, 47%, and 3% at the laser powers of 1.68, 1.30, and 0.89 W, respectively. Note that the contributions by plasmonic photocatalysis are underestimated. Under the laser illumination, the temperature of the reaction solution rose gradually from room temperature to the end temperature. The rise took ∼20 min. In contrast, under the isothermal heating, the water bath was preset at the desired temperature. It took less than 1 min for the solution temperature to become equilibrated with that of the water bath. For example, if the reactant solution and the catalyst solution were both preheated to 56 °C, mixed together, and then subjected to the laser illumination at 1.30 W for 20 min, the yield became 80%.

3.3.2. Photocatalysis (−) and Photothermal Heating (+). Two types of nanostructures were prepared to turn off plasmonic photocatalysis under the 809 nm laser illumination while maintaining photothermal heating. The contribution of plasmonic photocatalysis under on- and off-resonance excitation conditions was first examined. We assumed that off-resonance illumination will give less hot electrons or the energy of the excited electrons will not be high enough for accelerating the reaction. The spherical Au−Pd nanostructures (Figure 3) with a plasmon wavelength of 526 nm were employed, and the results were compared with those of the large nanostructures. The spherical nanostructures have an average diameter of 35 ± 3 nm. The Au cores are single-crystalline, and the Pd nanoparticles are probably grown heteroepitaxially on the Au cores, as revealed by ED and high-resolution (HR)TEM characterizations (Figure S5, Supporting Information). The extinction value of the reaction solution containing the spherical nanostructures is 0.33 at 809 nm (Figure 3G). At the laser power of 1.30 W, only 7% of bromobenzene was converted, and the end temperature was 44 °C (Figure 3H and Table 3). When the laser power was raised

Table 3. Yields of the Suzuki Coupling Reaction between Bromobenzene and *m*-Tolylboronic Acid in the Presence of the Spherical Au−Pd Nanostructures[a]

laser power (W)	end temperature (°C)	yield (%)
2.06	59	34
1.30	44	7

[a]Environmental temperature, 25 °C; reaction time, 20 min.

to 2.06 W to make the end temperature comparable to those obtained with the large Au−Pd nanostructures, the reached end temperature was 59 °C, and the reaction yield was 34%. In comparison, the yield was 54% when the reaction solution containing the spherical nanostructures was heated in the water bath to 59 °C.

Two observations can be made from these control experiments. First, at comparable laser powers, the reaction yields under the on-resonance excitation are much larger than those under the off-resonance excitation. Second, at comparable end temperatures under the laser illumination, the yields under the on-resonance excitation are larger than those under the off-

resonance excitation. Besides the comparison between the on- and off-resonance experiments, we also found that the yields under the off-resonance excitation are smaller than those under the isothermal heating when the end temperature of the former is equal to the temperature of the isothermal heating. We believe that the lower yields under the off-resonance excitation than those under the isothermal heating are caused by the rapid thermal equilibration between the reaction solution and the water bath in comparison to the gradual temperature rise under the off-resonance excitation. This result confirms our assumption that the contribution of plasmonic photocatalysis under off-excitation condition to the reaction activity is very small.

Second, we prepared the nanostructures with a 25-nm-thick TiO$_x$ shell placed in between the Au core and Pd nanoparticles in order to prevent the electron transfer between the two metals (Figure 4). The use of TiO$_x$ as the separating layer is because SiO$_2$ can be dissolved in the basic Suzuki coupling reaction solutions. The 809 nm laser can only excite the electron oscillations on the Au nanorod core. The hot electron effect is then prohibited. The average diameter and length of the Au−TiO$_x$ core−shell nanostructures are 80 ± 6 nm and 137 ± 11 nm, respectively. The average thickness of the TiO$_x$ shell at the end and the side are 26 ± 7 nm and 26 ± 6 nm. Pd nanoparticles are grown and attached on the surface of the TiO$_x$ shell, as revealed by TEM, HAADF-STEM, and elemental mapping characterizations (Figure 4). The average size of the Pd nanoparticles is 16 ± 5 nm. We also prepared four additional nanostructure samples with different amounts of the Pd seeds and H$_2$PdCl$_4$. The extinction spectra of all the five nanostructure samples are nearly the same (Figure S6A, Supporting Information). The spectral shapes are also the same as that of the Au−TiO$_x$ core−shell nanostructure sample. Only the intensity is reduced, which is caused by the sample loss during the multistep washing process. The extinction results show that the plasmon coupling between the Au nanorod core and the Pd nanoparticles is very weak or nonexistent, because our previous studies show that the plasmon resonance of Au nanorods is extremely sensitive to the presence of Pd nanoparticles on the nanorod surface.[52] In addition, our XRD measurement (Figure S6B, Supporting Information) indicates that the TiO$_x$ shell is amorphous. This is consistent with the preparation procedure, which is performed at room temperature and involves no thermal treatment. The amorphous nature of the TiO$_x$ shell precludes the electron transfer between the Au core and the Pd nanoparticles. The weak or nonexistent plasmon coupling, together with the large imaginary part of the dielectric function of palladium, implies that the plasmon resonance in the Pd nanoparticles is very weak.

The catalytic activities of the large Au−Pd and Au−TiO$_x$−Pd nanostructures in the isothermal water bath were compared. The amount of the Au−TiO$_x$−Pd nanostructures was varied in order to obtain the same catalytic activity as that of the large Au−Pd nanostructures. A yield of 35% was obtained at 56 °C for 20 min with 0.5 mL of the Au−TiO$_x$−Pd nanostructure solution. The reaction solution was found by ICP-OES to contain 107 µg of Au and 10 µg of Pd. The yield was very close to that given by the large Au−Pd nanostructures. The latter was 37%. Therefore, the catalytic activities of the two nanostructure samples under isothermal heating were tuned to be very close. The extinction value of the reaction solution containing the Au−TiO$_x$−Pd nanostructures was 3.1 at 809 nm (Figure 4H).
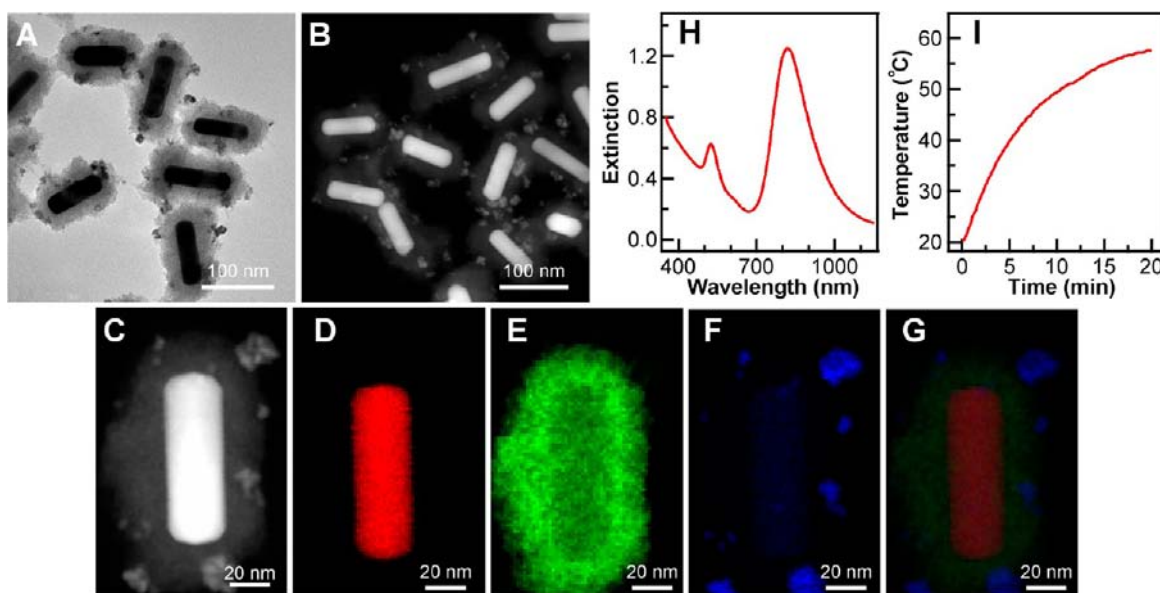
Figure 4. Au−TiO$_x$−Pd nanostructures. (A) TEM image. (B) HAADF-STEM image. (C) HAADF-STEM image of a single nanostructure. (D) Elemental map of gold of the nanostructure shown in C. (E) Corresponding elemental map of titanium. (F) Corresponding elemental map of palladium. (G) Merged elemental map. (H) Extinction spectrum. The reaction solution was diluted 2.5 times for the extinction measurement. The extinction value at 809 nm is 1.23 at a 1 cm path length. (I) Temperature rise trace of the reaction solution containing the Au−TiO$_x$−Pd nanostructures at 1.30 W of the 809 nm laser. The temperatures were measured at a time interval of 5 s. Therefore the trace is shown as a line.

At a laser power of 1.30 W, only 19% of bromobenzene was converted, and the end temperature was 58 °C (Figure 4I and Table 4). The photothermal conversion efficiency of the Au−

Table 4. Yields of the Suzuki Coupling Reaction between Bromobenzene and *m*-Tolylboronic Acid in the Presence of the Au−TiO$_x$−Pd Nanostructures[a]

start temperature (°C)	end temperature (°C)	yield (%)
21	58	19
56	58	39

[a]Laser power, 1.30 W; environmental temperature, 21 °C; reaction time, 20 min.

TiO$_x$−Pd nanostructures was determined to be 87%. In comparison, the yield of the reaction with the large Au−Pd nanostructures at the same laser power was 70% and the end temperature of the reaction solution was 56 °C (Table 2). Moreover, when the temperature of the reaction solution containing the Au−TiO$_x$−Pd nanostructures was preheated to 56 °C and the solution was illuminated at 1.30 W for 20 min, the reaction yield was 39%, which is close to that (35%) of the reaction with the Au−TiO$_x$−Pd nanostructures and that (37%) with the large Au−Pd nanostructures in the isothermal water bath at 56 °C without laser illumination.

The results above clearly suggest that the Au−TiO$_x$−Pd nanostructures only possess the photothermal heating effect while the Au−Pd nanostructures have both the plasmonic photocatalysis and photothermal heating effects for the Suzuki coupling reactions. The plasmonic heating and water-bath heating show very similar effects for the catalytic reaction. Although the direct evidence of the electron transfer from the metal to the adsorbed molecules remains to be unraveled, the comparison of the catalytic activities between the Au−TiO$_x$−Pd and Au−Pd nanostructures confirms the role of plasmonic photocatalysis in catalytic chemical reactions.

3.3.3. Photocatalysis (+) and Photothermal Heating (−). Two water baths set at relatively low temperatures were utilized to minimize the photothermal heating effect. The heat generated by plasmonic photothermal conversion was quickly dissipated into the water baths. One bath was made from ice water, and the other was set at 21 °C. Under the laser illumination at 1.30 W, the temperature of the reaction solution in the ice−water bath increased to and stayed at 2 °C. The reaction yield was 1.23% after 1 h under the laser illumination and 0 without the laser illumination. For the reaction in the bath set at 21 °C, the temperature slightly increased to and stayed at 24 °C under the laser illumination at 1.30 W. Only 6% of bromobenzene was converted in 1 h. The yield dropped to <1% when the bath was set at 24 °C, and no laser illumination was applied. The reaction was severely retarded by the low temperature. We therefore doubled the amount ratio between the catalyst and bromobenzene and prolonged the reaction time to 3 h in order to facilitate the comparison of the catalytic activities. As a result, 83% of bromobenzene was converted under the laser illumination in the water bath set at 21 °C, which a yield of 7% was obtained in the bath at 24 °C without the laser illumination. According to the estimation given below, the temperature of the reaction solution is nearly equal to that on the surface of the metal nanostructure. Therefore, at the low temperature, plasmonic photothermal heating is switched off. The catalytic conversions around room temperature are dominantly contributed by plasmonic photocatalysis through hot electrons.

3.3.4. Photocatalysis (−) and Photothermal Heating (−). When the catalytic reaction was run at room temperature (21 °C) without the laser illumination for 20 min, the reaction yield was below 1%. Because the laser illumination was blocked, both plasmonic photocatalysis and photothermal conversion were switched off. Therefore, the reaction was severely blocked.

3.4. Estimation of the Surface and Hot-Electron Temperatures of the Metal Nanostructures under the

Laser Illumination. We estimated the temperature difference between the surface of the Au−Pd nanostructures and the reaction solution by treating each nanostructure as a heat source and taking into account the illumination laser power, the absorption cross section, and the thermal conductivity of the aqueous solution. The estimation was made in order to ascertain whether there is a temperature difference on the surface of the metal nanostructures and the solution. Under continuous, low-power laser illumination, the temperature difference can be estimated according to the formula derived by Halas et al.[53]

$$\Delta T = \frac{\sigma_{abs} I}{4\pi R_{eq} \beta \kappa} \tag{1}$$

where σ_{abs} is the absorption cross section of the metal nanostructure, I is the intensity of the illumination laser, R_{eq} is the radius of the sphere of the same volume as the nanostructure, β is the thermal capacitance coefficient of the nanostructure, and κ is the thermal conductivity of the solution. β is dependent on the aspect ratio, AR, of the nanostructure according to

$$\beta = 1 + 0.96587[\ln^2(AR)] \tag{2}$$

The aspect ratios of the large and smallest Au−Pd nanostructures are 3.28 and 3.42, respectively. Their β values are therefore 2.3628 and 2.4604. Their R_{eq} values are 20.5 and 15.8 nm. The diameter of the laser spot in the solution is ∼0.33 cm. At the laser power of 2.06 W, I = 24.1 W·cm^{-2}. The thermal conductivity of the solution is taken as that of water, which is 0.58 W·(m·K)$^{-1}$. Therefore, the estimated ΔT values for the large and smallest Au−Pd nanostructures are 0.038 and 0.024 °C, respectively. For comparison, in the work of Halas et al., a ΔT of 1.5×10^{-4} K was obtained for Au nanorods of AR = 3.6 under a resonant laser power of I = 1.3 W·cm^{-2} in water.[53] Such small temperature differences allow us to exclude the contribution of the nonequilibrium thermal distribution to the enhanced catalytic activities of the Au−Pd nanostructures. Therefore, the temperature recorded from the reaction solution is indicative of the photothermal heating effect. We note that the temperature differences under pulsed laser excitation, owing to much higher laser power densities within each pulse, are generally much larger than those under low-power, continuous laser excitation,[54] because it takes time for the excited electrons to thermally equilibrate with the lattice phonons and for the lattice phonons to thermally equilibrate with the phonons in the surrounding environment.

Our studies presented above indicate that both plasmonic photocatalysis and photothermal heating play roles in the catalytic reactions. Their relative contributions are dependent on the incident laser power, the plasmon wavelength, and the presence or absence of a separating layer between the Au core and the Pd nanoparticles. At low laser powers, plasmonic photothermal conversion contributes dominantly. At high laser powers, more electrons are populated above the Fermi level due to the plasmon excitation. The contribution of plasmonic photocatalysis therefore becomes more important. In addition, the contribution of plasmonic photocatalysis is larger under on-resonance plasmon excitation than that under off-resonance excitation. An inert layer that separates the Au core and the Pd nanoparticles will block plasmonic photocatalysis. We would also mention that pure Au nanorods cannot catalyze the reaction under either the laser-illumination or isothermal-heating conditions due to the fact that Au nanocrystals with sizes above ∼10 nm cannot chemically adsorb the reactant molecules for the Suzuki coupling reactions. Therefore, electrons cannot be injected from the Au nanorod to the molecules. Our catalyst system is different from the one reported previously,[55] where Au nanoparticles themselves serve as the catalyst for alcohol oxidation reactions and an electron injection process is proposed.

For the coupling reaction between bromobenzene and m-tolylboronic acid, the rate-determining step is the breaking of the C−Br bond.[51] In the homogeneous catalysis with Pd complexes, this step is known as the oxidative addition, where Pd(0) is oxidized into Pd(II). There exists electron transfer from the Pd atom to the Br and C atoms. However, this step is complex and unclear in the heterogeneous catalysis, as in our study. We therefore performed DFT calculations on the C−Br bond dissociation reaction on the Pd (111) surface in order to simulate the process. The calculated activation energy is 0.76 eV (Figure S7, Supporting Information). The charge analysis indicated that the net charges on the two Pd atoms become more positive, the net charge on the Br atom turns from positive to negative, and that on the C atom becomes more negative during the C−Br dissociation reaction (Table S3, Supporting Information). This result implies that the rate-determining step in the heterocatalysis also involves the electron transfer from the Pd atoms to the Br and C atoms.

In order to further understand the effect of the plasmon-excitation-induced hot electrons on the reactions, we estimated the energy distribution of the hot electrons.[56] The electron−phonon relaxation time is between several tens of picoseconds to hundreds of picoseconds.[57] The lifetime of the hot electrons is then below one nanosecond. Excited by the 809 nm laser at 24.1 W·cm^{-2}, a large Au−Pd nanostructure receives an energy of 1.35×10^{-17} J in 1 ns. The heat capacity of the electron Fermi gas is

$$C_{el} = \frac{1}{2}\pi^2 N k_B \frac{T}{T_F} \tag{3}$$

where N is the number of the conduction-band electrons, k_B is the Boltzmann cnstant, and T_F is the Fermi temperature. T_F can be determined from

$$k_B T_F = E_F \tag{4}$$

and

$$E_F = \frac{\hbar^2}{2m}\left(\frac{3\pi^2 N}{V}\right)^{2/3} \tag{5}$$

where m is the mass of a free electron and V is the volume of the electron Fermi gas, that is, the volume of the metal nanostructure. In our case, a majority part of the Au−Pd nanostructure is gold. We then considered the gold component only to simplify the calculation. In our experiment, $V = 3.62 \times 10^4$ nm^3 and $N = 2.13 \times 10^6$. The calculated values of E_F and T_F for the large Au−Pd nanostructure are 8.84×10^{-19} J (5.52 eV) and 6.41×10^4 K, respectively. These values are very close to those of bulk gold, which are 5.51 eV and 6.39×10^4 K.[56] Therefore, $C_{el} = 6.75 \times 10^{-19}$ J·K^{-1} at 298 K. The temperature increase of the free electron gas within one nanosecond is 20 K. The temperature increase slightly drops to 17 K when the environment temperature is 343 K. These estimations show that the temperature of the hot electrons is always ∼20 K above the lattice temperature before the electron−phonon relaxation.

Therefore, the electrons upon the plasmon excitation have a better chance to inject into the adsorbed bromobenzene molecules. This temperature difference is very important for the Suzuki coupling reactions, which usually take place at 20−40 K above room temperature. This result explains why only 1.23% of bromobenzene was converted in 1 h for the reaction in the ice−water bath under the laser illumination. Under that condition, the temperature of the hot electrons was only ∼20 °C. The reaction was severely retarded at that temperature. The result also explains why the yields under off-resonance excitation were lower than those under on-resonance excitation. Under off-resonance excitation, the absorption cross-section of the spherical Au−Pd nanostructures at 809 nm was much smaller than that of the large Au−Pd nanostructures. The resultant temperature of the hot electrons was much lower and cannot accelerate the reactions.

We also examined the leaching of palladium. For the large Au−Pd nanostructures, 22%, 21%, and 21% of palladium were found to remain in the supernatants after 20 min of the reaction under the 809 nm laser illumination at 0.89, 1.30, and 1.68 W, respectively. For the Au−TiO$_x$−Pd nanostructures, 22% of palladium was leached after reaction for 20 min under the 809 nm laser illumination at 1.30 W. In our previous experiment of using porous Pd nanocrystals as the catalyst for the Suzuki coupling reaction, almost no Pd leaching was detected.[45] The difference can be attributed to the different metal nanostructures, the different reaction solvents, and the use of CTAB in the reaction solution in this study. To test the contribution of the leached palladium to the reaction, the supernatant of the reaction solution after 20 min under the 809 nm laser illumination at 1.30 W with the large Au−Pd nanostructures as the catalyst was divided into two aliquots. One aliquot was subjected to the GC-MS analysis, and the other was placed in a water bath at 56 °C for another 20 min. The reaction yields for the two aliquots were measured to be 70% and 81%, respectively. The yield difference of 11% is believed to result from the leached palladium. The leached palladium can be the Au−Pd nanostructures remaining in the supernatant or the dissolved Pd ions. The former will not affect our results on the relative contributions of plasmonic photocatalysis and photo-thermal conversion. The latter will increase the contribution of the plasmonic photothermal heating effect to the catalytic activity. Therefore, overall, the Pd leaching does not affect our analysis of the effect of plasmonic photocatalysis on the catalytic activity. Future experiments are required to tackle the Pd leaching problem so that the metal nanostructure catalysts are recyclable.

3.5. Size Effect. We investigated the size effect of the nanostructures on plasmon-enhanced reactions using the smallest Au−Pd nanostructures. The smallest and large nanostructure samples have a similar morphology, the same longitudinal plasmon wavelength, and nearly equal extinction values at the longitudinal plasmon peak (Figure 5). The average diameter and length of the smallest Au−Pd nanostructures are 19 ± 2 and 65 ± 5 nm, respectively. Its average particle volume is approximately half of that of the large Au−Pd nanostructures. The absorption cross sections of a single large and smallest nanostructure were calculated according to the average sizes on the basis of Gans theory by considering only gold.[39] They are 5.6 × 10^{-14} and 2.8 × 10^{-14} m^2 at 809 nm, respectively. The difference in their absorption cross sections comes from their different sizes.[38−40] The seven reactions that have product yields less than 99% in Table 1 were tested with the smallest
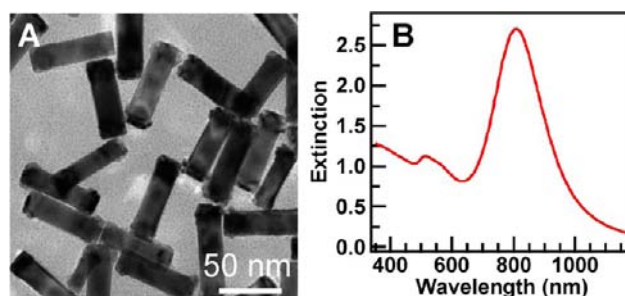
Figure 5. Smallest Au−Pd nanostructures. (A) TEM image. (B) Extinction spectrum of the reaction solution containing the nanostructures. The extinction value at 809 nm is 2.70 at a 1 cm path length.

Au−Pd nanostructures under the similar conditions. Higher product yields were obtained for all of the seven reactions (Table 5). Even the coupling reaction between o-bromoanisole

Table 5. Yields of the Suzuki Coupling Reactions in the Presence of the Smallest Au−Pd Nanostructures under the 809 nm Laser Illumination[a]

entry	halide	boronic acid	yield [%]
1	⬡—Br	CH$_3$—⬡—B(OH)$_2$	99
2	⬡—Br (OCH$_3$)	⬡—B(OH)$_2$ (CH$_3$)	99
3	⬡—Br (OCH$_3$)	⬡—B(OH)$_2$ (CH$_3$)	89
4	⬡—Br (OCH$_3$)	CH$_3$—⬡—B(OH)$_2$	99
5	⬡—Br (OCH$_3$)	⬡—B(OH)$_2$ (CH$_3$)	99
6	CH$_3$O—⬡—Br	⬡—B(OH)$_2$ (CH$_3$)	99
7	CH$_3$O—⬡—Br	⬡—B(OH)$_2$ (CH$_3$)	99

[a]Smallest Au−Pd nanostructure solution, 0.5 mL; NaOH, 10 mg; CTAB, 36 mg; H$_2$O, 1.5 mL; reactant amounts of entry 1, 0.08 mmol halide and 0.08 mmol boronic acid; reactant amounts of entries 2−7, 0.04 mmol halide and 0.04 mmol boronic acid; laser power, 1.68 W; environment temperature, 25 °C; reaction time, 1 h.

and o-tolylboronic acid reached a yield of 99% (Table 5, entry 2). These results indicate that smaller plasmonic nanostructures are more catalytically active under on-resonance laser illumination. Smaller metal nanostructures have been known to possess larger fractions of absorption in the total extinction.[39,46] Both plasmonic photocatalysis and photo-thermal conversion originate from the light absorption by metal nanostructures. As a result, a larger contribution of the absorption to the total extinction will lead to a greater enhancement in the catalytic activity.
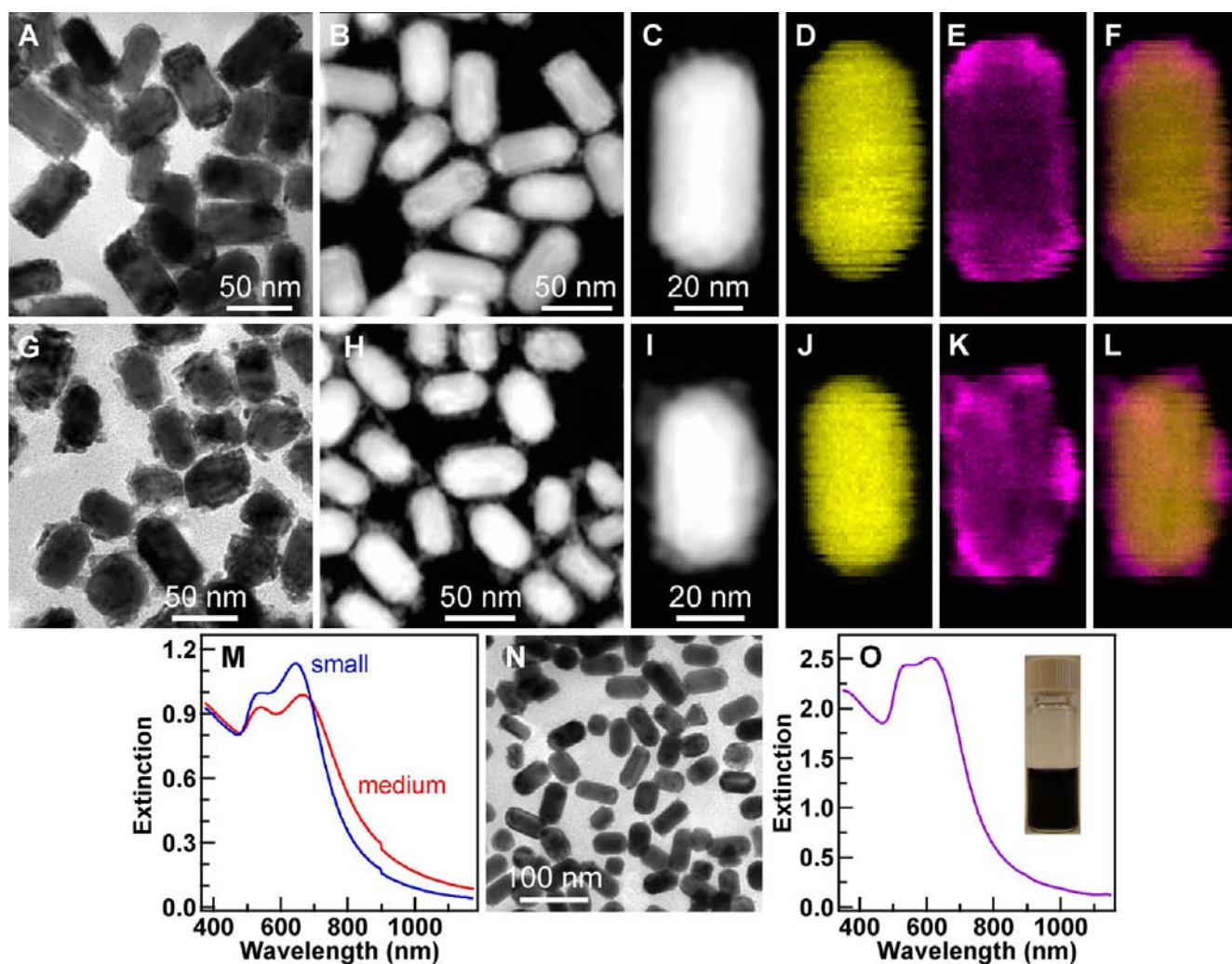
Figure 6. Nanostructures for the catalytic reactions under solar radiation. (A−F) Medium Au−Pd nanostructures: (A) TEM image; (B) HAADF-STEM image; (C) HAADF-STEM image of a single nanostructure; (D) elemental map of gold for the nanostructure shown in C; (E) corresponding elemental map of palladium; (F) merged elemental map. (G−L) Corresponding imaging results for the small Au−Pd nanostructures. (M) Extinction spectra recorded with 0.5 cm cuvettes for the medium and small Au−Pd nanostructure samples. (N) TEM image of the mixture of the medium, small, and spherical nanostructure samples. (O) Extinction spectrum of the mixture at 1 cm path length. The inset shows the digital photo of the reaction solution containing the nanostructure mixture in a glass vessel for the experiments under solar radiation.
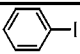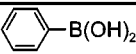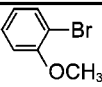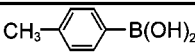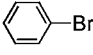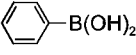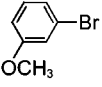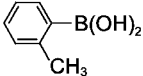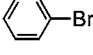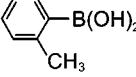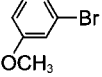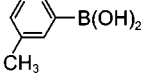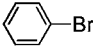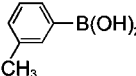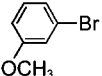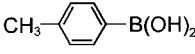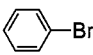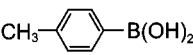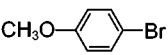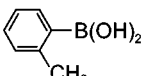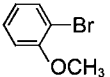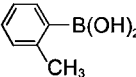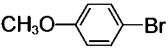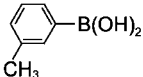
3.6. Suzuki Coupling Reactions under Sunlight. The Suzuki coupling reactions performed under the laser illumination suggest clearly the feasibility of utilizing light energy for chemical reactions with our Au−Pd nanostructures. On the basis of the obtained results, we set about examining the capability of the nanostructures to catalyze the reactions by directly harvesting solar energy. In order to maximize the absorption of sunlight, we mixed together the medium, small, and spherical Au−Pd nanostructures (Figure 6). Their main plasmon wavelengths are 677, 644, and 526 nm, respectively (Figures 6M and 3G). The average diameters/lengths of the medium and small nanostructures are $30 \pm 3/61 \pm 6$ and $30 \pm 3/53 \pm 5$, respectively. The ED patterns and HRTEM images (Figures S8 and S9, Supporting Information) also show that the medium and small nanostructures are single-crystalline, with Pd nanoparticles grown heteroepitaxially. The mixture sample (Figure 6N) looks black (Figure 6O, inset). It exhibits large extinction values over the spectral range from 520 to 640 nm (Figure 6O). The extinction value increases toward the shorter-wavelength region, owing to the interband transitions of gold and palladium. In the longer-wavelength region, the extinction
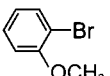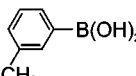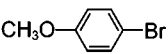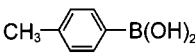
value decays to zero over the range of 640−1100 nm. The spectral region of the maximal extinction values for the mixture sample overlaps with that of the maximal radiation intensities for the solar spectrum. If we assume a depth of the mixture sample solution at 1 cm, 70% of sunlight interacts with the Au−Pd nanostructures in the solution on the basis of the AM1.5 reference spectrum (ASTMG173-03, direct normal + circumsolar). This value can be further improved by optimizing the morphology of the metal nanostructures.

We first tested the catalytic activity of the nanostructure mixture under solar radiation with the coupling reaction between bromobenzene and *m*-tolylboronic acid. Due to the lower intensity of sunlight than that of the laser, the reaction periods of time were extended to 2 h. The nanostructure mixture gave a yield of 99% under solar radiation.

In order to verify the role of the plasmon on the catalytic activity, three control experiments under solar radiation were performed. First, the same reaction solution was prepared in another vial. The vial was wrapped with aluminum foil. Under solar radiation for 2 h, only a yield of 5.3% was obtained. This nonzero yield is ascribed to the slight heating from the

Table 6. Yields of the Suzuki Coupling Reactions in the Presence of the Mixture of the Medium, Small, and Spherical Au–Pd Nanostructures under Solar Radiation[a]

entry	halide	boronic acid	yield [%]	entry	halide	boronic acid	yield [%]
1	⟨⟩–I	⟨⟩–B(OH)₂	97	8	⟨⟩–Br, OCH₃	CH₃–⟨⟩–B(OH)₂	70
2	⟨⟩–Br	⟨⟩–B(OH)₂	99	9	⟨⟩–Br, OCH₃	⟨⟩–B(OH)₂, CH₃	99
3	⟨⟩–Br	⟨⟩–B(OH)₂, CH₃	99	10	⟨⟩–Br, OCH₃	⟨⟩–B(OH)₂, CH₃	99
4	⟨⟩–Br	⟨⟩–B(OH)₂, CH₃	96	11	⟨⟩–Br, OCH₃	CH₃–⟨⟩–B(OH)₂	99
5	⟨⟩–Br	CH₃–⟨⟩–B(OH)₂	99	12	CH₃O–⟨⟩–Br	⟨⟩–B(OH)₂, CH₃	99
6	⟨⟩–Br, OCH₃	⟨⟩–B(OH)₂, CH₃	50	13	CH₃O–⟨⟩–Br	⟨⟩–B(OH)₂, CH₃	76
7	⟨⟩–Br, OCH₃	⟨⟩–B(OH)₂, CH₃	67	14	CH₃O–⟨⟩–Br	CH₃–⟨⟩–B(OH)₂	55

[a]Au–Pd nanostructure mixture solution, 1 mL; NaOH, 10 mg; CTAB, 36 mg; H₂O, 1 mL; reactant amounts of entries 1–5, 0.08 mmol halide and 0.08 mmol boronic acid; reactant amounts of entries 6–14, 0.04 mmol halide and 0.04 mmol boronic acid; solar power, 565 W·m⁻²; environment temperature, 30 °C; reaction time, 2 h.

surrounding environment. Second, we mixed together the porous Pd nanocrystals and the three Au nanocrystal samples that were used for the preparation of the medium, small, and spherical Au–Pd nanostructure samples (Figure S10, Supporting Information) and tested the catalytic activity of the resultant mixture. The Au and Pd molar compositions were adjusted to be the same. A yield of 16% was obtained under solar radiation. This yield results from the plasmonic photothermal heating of the Au nanocrystals in the solution. The result shows again the importance of the integration of plasmonic and catalytic components for the efficient utilization of light energy. Third, during the reaction under solar radiation, the temperature of the reaction solution reached 38 °C after 2 h (Figure S11, Supporting Information). We performed the same catalytic reaction using the same Au–Pd nanostructure mixture under isothermal heating at temperatures of 35, 40, and 45 °C, because there was fluctuations in the environmental temperature under solar radiation. The obtained reaction yields were 34%, 58%, and 70%, respectively. These yields are lower than that obtained under solar radiation. Owing to the broadband nature of solar irradiation, the quantitative contributions of the plasmonic photocatalysis and photothermal conversion to the higher yield remain to be further examined.

We finally carried out all of the 14 reactions that had been studied above under the laser illumination. Similarly, all of the reactions under solar radiation gave yields above 50%, with nine of them even above 90% (Table 6). The catalyst used in the solar-radiation experiments was estimated to contain 326 μg of gold and 16.6 μg of palladium. The calculated TOFs are listed in Table S4 in the Supporting Information. The high reaction yields obtained under solar radiation points out the potential of

directly harvesting solar energy to overcome the energy barriers in chemical reactions.

4. CONCLUSION

We demonstrated the harvesting of light energy for chemical reactions using Au–Pd nanostructures made of Au nanocrystal cores and tightly bonded Pd nanoparticles. The Au nanocrystal core acts as a plasmonic component for efficient light absorption, and the Pd nanoparticles act as the catalysts for Suzuki coupling reactions. The intimate integration of plasmonic and catalytic components in one nanostructure allows the light energy absorbed by the plasmonic component to be directly transferred to the catalytic component. Both plasmonic photocatalysis and photothermal heating contribute to the catalytic activity. The contribution of plasmonic photocatalysis was confirmed by comparing the activities between the Au–Pd and Au–TiO$_x$–Pd nanostructures. The DFT calculations and theoretical estimation suggest the probability of the hot electron injection from the Pd surface to the adsorbed bromobenzene molecules. The contribution of plasmonic photocatalysis was found to be dependent on the incident laser power, the plasmonic wavelength, the separating layer between the Au core and the Pd nanoparticles, the environmental temperature, and the size of the nanostructures. The Au–Pd nanostructures were further synthetically tailored to directly harvest sunlight for the catalytic reactions. Our design of the plasmonic–catalytic hybrid nanostructures and catalytic results suggest a potential means for the direct utilization of sunlight for a variety of industrially important catalytic reactions.

■ ASSOCIATED CONTENT

Ⓢ Supporting Information

The elemental mapping of a single large Au−Pd nanostructure, reaction setup, extinction spectra of the nanostructures and their mixtures, extinction spectra and XRD pattern of the Au−TiO$_x$−Pd nanostructures, reaction coordinate of the rate-determining step, TEM images of the porous Pd nanocrystals, TEM images, ED patterns, and HRTEM images of the spherical, medium, and small Au−Pd nanostructures, temperature rise trace of the reaction solution under solar radiation, reaction yields under the isothermal heating, TOFs of the reactions under the laser illumination and solar radiation, and net charges on the atoms involved in the rate-determining step at the initial, transition, and final states. This material is available free of charge via the Internet at http://pubs.acs.org.

■ AUTHOR INFORMATION

Corresponding Author

jfwang@phy.cuhk.edu.hk; sun@pku.edu.cn; yan@pku.edu.cn

Notes

The authors declare no competing financial interest.

■ ACKNOWLEDGMENTS

■ REFERENCES

(1) Lewis, N. S.; Nocera, D. G. *Proc. Natl. Acad. Sci. U.S.A.* **2006**, *103*, 15729−15735.

(2) Lewis, N. S. *MRS Bull.* **2007**, *32*, 808−820.

(3) Shah, A.; Torres, P.; Tscharner, R.; Wyrsch, N.; Keppner, H. *Science* **1999**, *285*, 692−698.

(4) Gust, D.; Moore, T. A.; Moore, A. L. *Acc. Chem. Res.* **2001**, *34*, 40−48.

(5) Blankenship, R. E.; Tiede, D. M.; Barber, J.; Brudvig, G. W.; Fleming, G.; Ghirardi, M.; Gunner, M. R.; Junge, W.; Kramer, D. M.; Melis, A.; Moore, T. A.; Moser, C. C.; Nocera, D. G.; Nozik, A. J.; Ort, D. R.; Parson, W. W.; Prince, R. C.; Sayre, R. T. *Science* **2011**, *332*, 805−809.

(6) Kudo, A.; Miseki, Y. *Chem. Soc. Rev.* **2009**, *38*, 253−278.

(7) Kubacka, A.; Fernández-García, M.; Colón, G. *Chem. Rev.* **2012**, *112*, 1555−1614.

(8) Linic, S.; Christopher, P.; Ingram, D. B. *Nat. Mater.* **2011**, *10*, 911−921.

(9) Ming, T.; Chen, H. J.; Jiang, R. B.; Li, Q.; Wang, J. F. *J. Phys. Chem. Lett.* **2012**, *3*, 191−202.

(10) Watanabe, K.; Menzel, D.; Nilius, N.; Freund, H.-J. *Chem. Rev.* **2006**, *106*, 4301−4320.

(11) Knight, M. W.; Sobhani, H.; Nordlander, P.; Halas, N. J. *Science* **2011**, *332*, 702−704.

(12) Thomann, I.; Pinaud, B. A.; Chen, Z. B.; Clemen, B. M.; Jaramillo, T. F.; Brongersma, M. L. *Nano Lett.* **2011**, *11*, 3440−3446.

(13) Liu, Z. W.; Hou, W. B.; Pavaskar, P.; Aykol, M.; Cronin, S. B. *Nano Lett.* **2011**, *11*, 1111−1116.

(14) Qu, Y. Q.; Cheng, R.; Su, Q.; Duan, X. F. *J. Am. Chem. Soc.* **2011**, *133*, 16730−16733.

(15) Ingram, D. B.; Linic, S. *J. Am. Chem. Soc.* **2011**, *133*, 5202−5205.

(16) Cushing, S. K.; Li, J. T.; Meng, F. K.; Senty, T. R.; Suri, S.; Zhi, M. J.; Li, M.; Bristow, A. D.; Wu, N. Q. *J. Am. Chem. Soc.* **2012**, *134*, 15033−15041.

(17) Silva, C. G.; Juárez, R.; Marino, T.; Molinari, R.; García, H. *J. Am. Chem. Soc.* **2011**, *133*, 595−602.

(18) Naya, S.; Inoue, A.; Tada, H. *J. Am. Chem. Soc.* **2010**, *132*, 6292−6293.

(19) Kowalska, E.; Mahaney, O. O. P.; Abe, R.; Ohtani, B. *Phys. Chem. Chem. Phys.* **2010**, *12*, 2344−2355.

(20) Tanaka, A.; Hashimoto, K.; Kominami, H. *Chem. Commun.* **2011**, *47*, 10446−10448.

(21) Zhai, W. Y.; Xue, S. J.; Zhu, A. W.; Luo, Y. P.; Tian, Y. *ChemCatChem* **2011**, *3*, 127−130.

(22) Chen, X.; Zhu, H.-Y.; Zhao, J.-C.; Zheng, Z.-F.; Gao, X.-P. *Angew. Chem., Int. Ed.* **2008**, *47*, 5353−5356.

(23) Zhu, H. Y.; Ke, X. B.; Yang, X. Z.; Sarina, S.; Liu, H. W. *Angew. Chem., Int. Ed.* **2010**, *49*, 9657−9661.

(24) Christopher, P.; Xin, H. L.; Linic, S. *Nat. Chem.* **2011**, *3*, 467−472.

(25) Yen, C.-W.; El-Sayed, M. A. *J. Phys. Chem. C* **2009**, *113*, 19585−19590.

(26) Adleman, J. R.; Boyd, D. A.; Goodwin, D. G.; Psaltis, D. *Nano Lett.* **2009**, *9*, 4417−4423.

(27) Boyer, D.; Tamarat, P.; Maali, A.; Lounis, B.; Orrit, M. *Science* **2002**, *297*, 1160−1163.

(28) Richardson, H. H.; Hickman, Z. N.; Govorov, A. O.; Thomas, A. C.; Zhang, W.; Kordesch, M. E. *Nano Lett.* **2006**, *6*, 783−788.

(29) Jain, P. K.; Huang, X. H.; El-Sayed, I. H.; El-Sayed, M. A. *Acc. Chem. Res.* **2008**, *41*, 1578−1586.

(30) Lal, S.; Clare, S. E.; Halas, N. J. *Acc. Chem. Res.* **2008**, *41*, 1842−1851.

(31) Rycenga, M.; Wang, Z. P.; Gordon, E.; Cobley, C. M.; Schwartz, A. G.; Lo, C. S.; Xia, Y. N. *Angew. Chem., Int. Ed.* **2009**, *48*, 9924−9927.

(32) Hasan, W.; Stender, C. L.; Lee, M. H.; Nehl, C. L.; Lee, J.; Odom, T. W. *Nano Lett.* **2009**, *9*, 1555−1558.

(33) Fang, C. H.; Shao, L.; Zhao, Y. H.; Wang, J. F.; Wu, H. K. *Adv. Mater.* **2012**, *24*, 94−98.

(34) Hung, W. H.; Aykol, M.; Valley, D.; Hou, W. B.; Cronin, S. B. *Nano Lett.* **2010**, *10*, 1314−1318.

(35) Yin, L. X.; Liebscher, J. *Chem. Rev.* **2007**, *107*, 133−173.

(36) Bing, Y. H.; Liu, H. S.; Zhang, L.; Ghosh, D.; Zhang, J. J. *Chem. Soc. Rev.* **2010**, *39*, 2184−2202.

(37) Balanta, A.; Godard, C.; Claver, C. *Chem. Soc. Rev.* **2011**, *40*, 4973−4985.

(38) Murphy, C. J.; Sau, T. K.; Gole, A. M.; Orendorff, C. J.; Gao, J. X.; Gou, L. F.; Hunyadi, S. E.; Li, T. *J. Phys. Chem. B* **2005**, *109*, 13857−13870.

(39) Ni, W. H.; Kou, X. S.; Yang, Z.; Wang, J. F. *ACS Nano* **2008**, *2*, 677−686.

(40) Jain, P. K.; Lee, K. S.; El-Sayed, I. H.; El-Sayed, M. A. *J. Phys. Chem. B* **2006**, *110*, 7238−7248.

(41) Wang, F.; Sun, L.-D.; Feng, W.; Chen, H. J.; Yeung, M. H.; Wang, J. F.; Yan, C.-H. *Small* **2010**, *6*, 2566−2575.

(42) Wang, F.; Li, C. H.; Sun, L.-D.; Wu, H. S.; Ming, T.; Wang, J. F.; Yu, J. C.; Yan, C.-H. *J. Am. Chem. Soc.* **2011**, *133*, 1106−1111.

(43) Hu, J.-W.; Li, J.-F.; Ren, B.; Wu, D.-Y.; Sun, S.-G.; Tian, Z.-Q. *J. Phys. Chem. C* **2007**, *111*, 1105−1112.

(44) Liu, R.; Sen, A. *J. Am. Chem. Soc.* **2012**, *134*, 17505−17512.

(45) Wang, F.; Li, C. H.; Sun, L.-D.; Xu, C.-H.; Wang, J. F.; Yu, J. C.; Yan, C.-H. *Angew. Chem., Int. Ed.* **2012**, *51*, 4872−4876.

(46) Chen, H. J.; Shao, L.; Ming, T.; Sun, Z. H.; Zhao, C. H.; Yang, B. C.; Wang, J. F. *Small* **2010**, *6*, 2272−2280.

(47) Monkhorst, H. J.; Pack, J. D. *Phys. Rev. B* **1976**, *13*, 5188−5192.

(48) Halgren, T. A. *Chem. Phys. Lett.* **1977**, *49*, 225−232.

(49) Tsung, C.-K.; Kou, X. S.; Shi, Q. H.; Zhang, J. P.; Yeung, M. H.; Wang, J. F.; Stucky, G. D. *J. Am. Chem. Soc.* **2006**, *128*, 5352−5353.

(50) Miyaura, N.; Suzuki, A. *Chem. Rev.* **1995**, *95*, 2457−2483.

(51) Smith, G. B.; Dezeny, G. C.; Hughes, D. L.; King, A. O.; Verhoeven, T. R. *J. Org. Chem.* **1994**, *59*, 8151−8156.

(52) Chen, H. J.; Wang, F.; Li, K.; Woo, K. C.; Wang, J. F.; Li, Q.; Sun, L.-D.; Zhang, X. X.; Lin, H.-Q.; Yan, C.-H. *ACS Nano* **2012**, *6*, 7162−7171.

(53) Huschka, R.; Zuloaga, J.; Knight, M. K.; Brown, L. V.; Nordlander, P.; Halas, N. J. *J. Am. Chem. Soc.* **2011**, *133*, 12247−12255.

(54) Fasciani, C.; Bueno Alejo, C. J.; Grenier, M.; Netto-Ferreira, J. C.; Scaiano, J. C. *Org. Lett.* **2011**, *13*, 204−207.

(55) Hallett-Tapley, G. L.; Silvero, M. J.; González-Béjar, M.; Grenier, M.; Netto-Ferreira, J. C.; Scaiano, J. C. *J. Phys. Chem. C* **2011**, *115*, 10784−10790.

(56) Kittel, C. *Introduction to Solid State Physics*, 8th ed.; John Wiley & Sons: New York, 2005; pp 137−145.

(57) Link, S.; Burda, C.; Nikoobakht, B.; El-Sayed, M. A. *J. Phys. Chem. B* **2000**, *104*, 6152−6163.